

---

# Marginalization Consistent Probabilistic Forecasting of Irregular Time Series via Mixture of Separable flows

---

**Vijaya Krishna Yalavarthi\***  
 ISMLL  
 University of Hildesheim  
 Germany  
 yalavarthi@ismll.de

**Randolf Scholz\***  
 ISMLL  
 University of Hildesheim  
 Germany  
 scholz@ismll.de

**Christian Kloetgens**  
 ISMLL  
 University of Hildesheim  
 Germany  
 kloetgens@ismll.de

**Kiran Madhusudhanan**  
 ISMLL  
 University of Hildesheim  
 Germany  
 madhusudhanan@ismll.de

**Stefan Born**  
 Institute of Mathematics  
 TU Berlin  
 Germany  
 born@math.tu-berlin.de

**Lars Schmidt-Thieme**  
 ISMLL  
 University of Hildesheim  
 Germany  
 schmidt-thieme@ismll.de

## Abstract

Probabilistic forecasting models for joint distributions of targets in irregular time series with missing values are a heavily under-researched area in machine learning with, to the best of our knowledge, only two models are researched so far: the Gaussian Process Regression model (Dürichen et al., 2015), and ProFITi (Yalavarthi et al., 2024b). While ProFITi, thanks to using multivariate normalizing flows, is very expressive, leading to better predictive performance, it suffers from marginalization inconsistency: it does not guarantee that the marginal distributions of a subset of variables in its predictive distributions coincide with the directly predicted distributions of these variables. When asked to directly predict marginal distributions, they are often vastly inaccurate. We propose MOSES (Marginalization Consistent Mixture of Separable Flows), a model that parametrizes a stochastic process through a mixture of several latent multivariate Gaussian Processes combined with separable univariate Normalizing Flows. In particular, MOSES can be analytically marginalized allowing it to directly answer a wider range of probabilistic queries than most competitors. Experiments on four datasets show that MOSES achieves both accurate joint and marginal predictions, surpassing all other marginalization consistent baselines, while only trailing slightly behind ProFITi in joint prediction, but vastly superior when predicting marginal distributions.

## 1 Introduction

In domains like weather and healthcare time series data is uneven: variables arrive at irregular intervals, channels are observed independently leading to extremely sparse time series when aligned. While point prediction is the norm, many decision making applications require full probabilistic forecasts that capture uncertainty of possible outcomes. To address this, researchers have developed

probabilistic forecasting models for irregular time series (De Brouwer et al., 2019; Deng et al., 2020; Biloš et al., 2021; Schirmer et al., 2022). However, these models typically focus on univariate forecasts at single time points.

Yet many practical decisions ranging from diagnosing diseases to predicting weather depend on interactions between multiple variables over time, requiring accurate forecasts of joint multivariate distributions. This area remains underexplored, with only two notable models: Gaussian Process Regression (GPR) (Dürichen et al., 2015), which models multivariate Gaussians, and ProFITi (Yalavarthi et al., 2024b), which uses normalizing flows for greater flexibility. ProFITi achieves stronger performance but lacks a key property: marginalization consistency which guarantees that marginal distributions are the same whether queried directly or derived from the joint.

This consistency is crucial with varying numbers of observed variables. For instance, users ask a weather model for the probability of next three sunny days in San Diego and the chance of rain tomorrow. If the answers contradict each other, trust in the model erodes—even if prediction of three sunny days is accurate. In practice, we find that ProFITi, despite producing strong joint distributions, fails to maintain consistent marginals. On the other hand, GPR, while consistent, underperforms overall.

From this starting point we constructed a novel model that combines the ideas of Gaussian Processes, normalizing flows and mixture models in a way completely different from ProFITi and GPR, to achieve both, guaranteed marginalization consistency and high predictive accuracy (see Figure 3). Overall our contributions as follows:

1. We formalize the underexplored property of marginalization consistency in probabilistic forecasting for irregular time series (Section 2). We propose Wasserstein Distance based metric to measure the marginalization inconsistency (Section 6.1).
2. We introduce a novel probabilistic forecasting model for irregular time series, **Marginalization Consistent Mixtures of Separable Flows** (MOSES). MOSES combines multiple normalizing flows with: (i) **Gaussian Processes with full covariance matrices** as source distributions (as opposed to the usual identity matrix), and (ii) a **separable** invertible transformation, applied independently per dimension rather than jointly. We formally prove that MOSES is guaranteed to be Marginalization Consistent (Sections 4 and 5).
3. In experiments on four datasets, we show that MOSES outperforms other state-of-the-art marginalization-consistent models in both multivariate joint and univariate marginal distributions. While its performance on joint distributions is comparable to or slightly below that of ProFITi, MOSES significantly surpasses ProFITi in univariate marginals (Section 6), demonstrating the advantage of Marginalization Consistency. Code available at [https://anonymous.4open.science/r/seperable\\_flows-BACC](https://anonymous.4open.science/r/seperable_flows-BACC)

## 2 Preliminaries

We use the triplet representation of an irregular time series  $X$ , which is a sequence of  $N$ -many triplets (Horn et al., 2020; Yalavarthi et al., 2024b):

$$X := \left( (t_n^{\text{OBS}}, c_n^{\text{OBS}}, v_n^{\text{OBS}}) \right)_{n=1:N} \in \text{Seq}(\mathcal{X}), \quad \mathcal{X} = \mathbb{R} \times \{1, \dots, C\} \times \mathbb{R} \quad (1)$$

where  $t_n^{\text{OBS}} \in \mathbb{R}$  is the observation time point, and  $v_n^{\text{OBS}} \in \mathbb{R}$  is the observed value in channel  $c_n^{\text{OBS}} \in \{1, \dots, C\}$ . A **time series query**  $Q$  is a sequence of  $K$ -many pairs:

$$Q := \left( (t_k^{\text{QRY}}, c_k^{\text{QRY}}) \right)_{k=1:K} \in \text{Seq}(\mathcal{Q}), \quad \mathcal{Q} = \mathbb{R} \times \{1, \dots, C\} \quad (2)$$

where  $t_k^{\text{QRY}}$  is the future time point and  $c_k^{\text{QRY}}$  is the queried channel. A **forecasting answer**  $y$  is a sequence of scalars:  $y = (y_1, \dots, y_K)$ , where  $y_k \in \mathbb{R}$  is the forecasted value in channel  $c_k^{\text{QRY}}$  at time  $t_k^{\text{QRY}}$ . Here,  $\text{Seq}(\mathcal{X})$  denotes the space of finite sequences over  $\mathcal{X}$ . All the query time points are after the observations:  $\min_{k=1:K} t_k^{\text{QRY}} > \max_{n=1:N} t_n^{\text{OBS}}$ .

**Requirements.** A marginalization consistent probabilistic irregularly sampled time series forecasting model must satisfy the following requirements:

**R1 Joint Multivariate Prediction.** The task of probabilistic irregular time series forecasting is to find a model  $\hat{p}$  that can predict the joint multivariate distribution  $\hat{p}(y | Q, X)$  of the answers  $y$ , given the query points  $Q$  and observed series  $X$ . Both the context  $N = |X|$  and the query length  $K = |Q|$  are allowed to be dynamic.

$$\begin{aligned} \hat{p}: \text{Seq}(\mathbb{R} \times \mathcal{Q}) \times \text{Seq}(\mathcal{X}) &\rightarrow \mathbb{R}_{\geq 0}, \\ (y, Q, X) &\mapsto \hat{p}(y_1, \dots, y_K | Q_1, \dots, Q_K, X_1, \dots, X_N) \end{aligned} \quad (3)$$

So that, for a given pair  $(Q, X)$ , the partial function  $(y_1, \dots, y_K) \mapsto \hat{p}(y_1, \dots, y_K | Q, X)$  realizes a probability density on  $\mathbb{R}^{|Q|}$ .

**R2 Permutation Invariance.** As the time stamp and channel-ID are included in each sample, the order of the samples does not matter, and hence any model prediction should be independent of the order of both the query or context:

$$\hat{p}(y | Q, X) = \hat{p}(y^\pi | Q^\pi, X^\tau), \quad \forall \pi \in S_{|Q|}, \tau \in S_{|X|} \quad (4)$$

**R3 Marginalization Consistency/Projection Invariance.** Predicting the joint density for the sub-query  $Q_{-k}$  given by removing the  $k$ -th item from  $Q$  should yield the same result as marginalizing the  $k$ -th variable from the complete query  $Q$ .

$$\hat{p}(y_{-k} | Q_{-k}, X) = \int_{\mathbb{R}} \hat{p}(y | Q, X) dy_k \quad (5)$$

This generalizes to any subset  $K_S \subseteq \{1, \dots, K\}$ .

For a model satisfying **R1-R3**, we will only have to marginalize if we try to validate the marginalization consistency. For this validation we added requirement **R3**. Yalavarthi et al. (2024b) discussed **R1** and **R2**, but did not consider **R3**. We argue that irregularly sampled time series is realization of a stochastic process and **R3** is a fundamental property of any model that mimics it.

**Theorem 2.1.** *Any model that satisfies **R1-R3** realizes an  $\mathbb{R}$ -valued stochastic process over the index set  $T = \mathbb{R} \times \{1, \dots, C\}$ .*

*Proof.* This is a direct application of Kolmogorov’s extension theorem (Øksendal, 2003)

Marginalization consistency provides performance guarantees: when querying a consistent model, that is known to be close to the ground truth for queries of size  $K$ , then it also produces predictions close to the ground truth for queries of size  $< K$ . This is a consequence of the data processing inequality (DPI; Murphy, 2022).

$$\begin{aligned} &D_{KL}\left(p(y_1, \dots, y_K | Q_1, \dots, Q_K, X) \mid \hat{p}(y_1, \dots, y_K | Q_1, \dots, Q_K, X)\right) \\ &\geq D_{KL}\left(p(y_1, \dots, y_{K-1} | Q_1, \dots, Q_{K-1}, X) \mid \hat{p}(y_1, \dots, y_{K-1} | Q_1, \dots, Q_{K-1}, X)\right) \quad (\mathbf{R3}) \end{aligned}$$

Hence, we expect marginalization consistent models to generalize better across query sizes. This is directly reflected by the experimental results in Table 1 and 2: models, that are not consistent, do not perform well on the marginal prediction task.

### 3 Related Work

There have been multiple works that deal with point forecasting of irregular time series (Ansari et al., 2023; Che et al., 2018; Chen et al., 2024; Yalavarthi et al., 2024a). In this work we deal with probabilistic forecasting of irregular time series. Models such as NeuralFlows (Biloš et al., 2021), GRU-ODE (De Brouwer et al., 2019), and CRU (Schirmer et al., 2022) predict only the marginal distribution for a single time stamp. Additionally, interpolation models like HetVAE (Shukla and Marlin, 2022) and Tripletformer (Yalavarthi et al., 2023) can also be applied for probabilistic forecasting. However, they also produce only marginal distributions. All the above models assume underlying distribution is Gaussian which is not the case for lots of real-world datasets. On the other hand, Gaussian Process Regression (GPR; Dürichen et al., 2015), and ProFITi (Yalavarthi et al., 2024b) can predict proper joint distributions. ProFITi is not marginalization consistent because of non-separable encoder and probabilistic component.

There have been works on models for tractable and consistent marginals for fixed number of variables such as tabular data. Probabilistic Circuits (Choi et al., 2020) create a sum-prod network on the

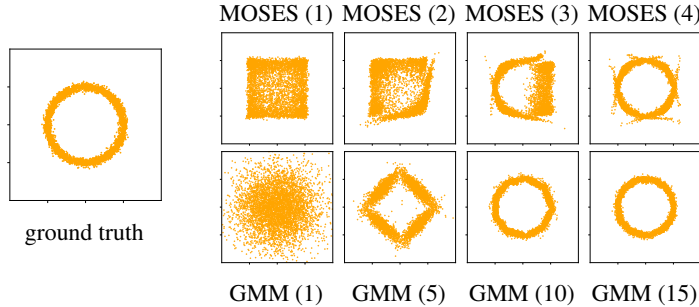


Figure 1: (Top) Importance of multiple flow components: MOSES(1) cannot represent the correct distribution, but MOSES(4) can. (Bottom) Limitation of Gaussian Mixture Models: GMM needs 15 components to match the distribution of MOSES(4).

marginal distributions in such a way that marginals are tractable and consistent. Later, Sidheekh et al. (2023) added univariate normalizing flows to the leaf nodes of the circuit for better expressivity. However, it is not trivial to extend such circuits to deal with sequential data of variable size. Gaussian Mixture Models (GMMs) (Duda and Hart, 1974) are often used only for unconditional density estimation, but can be extended to conditional density estimation. They can provide tractable and consistent marginal distributions. However, GMMs are not expressive enough and often require a very large number of components to approximate even simple distributions, see Figure 1. Note that normalizing flow models such as Dinh et al. (2017); Papamakarios et al. (2017, 2021) neither provide tractable marginals nor are applicable to varying number of variables.

Existing works have explored mixtures of normalizing flows for fixed-length sequences. For example, Pires and Figueiredo (2020) and Ciobanu (2021) used flows with affine coupling or masked autoregressive transformations for density estimation, while Postels et al. (2021) applied them to reconstruction tasks. However, these models cannot handle dynamic sequence lengths, and their marginals are intractable. Furthermore, there has been work non-Gaussian Gaussian Processes that use Normalizing Flows on top of Gaussian processes for few shot learning (Sendera et al., 2021) which is only capable of predicting a single variable/column, whereas our model is capable of predicting for multiple variables/columns, even under the presence of missing values.

## 4 Constructing Marginalization Consistent Conditional Distributions

Our goal is to build a model for the conditional joint distribution  $p(y_1, \dots, y_K | Q_1, \dots, Q_k, X)$ , as in Equation (3). Since the model should satisfy **R3**, it follows that the marginal distribution of  $y_k$  must only depend on  $Q_k$  and  $X$ .

**Separably Parametrized Gaussians.** The arguably most simple model for a permutation invariant conditional distribution for variably many variables is the family of multivariate Normal distributions  $\mathcal{N}(y | \mu(x), \Sigma(x))$ , whose conditional mean function  $\mu(x)$  and conditional covariance function  $\Sigma(x)$  are separable, i.e.:

$$\mu_k = \tilde{\mu}(Q_k, X) \quad \Sigma_{k,\ell} = \tilde{\Sigma}(Q_k, Q_\ell, X) \quad (6)$$

with mean function  $\tilde{\mu}$  and a covariance function  $\tilde{\Sigma}$ , a setup very well known from Gaussian processes. Such a separably parametrized multivariate Gaussian is marginalization consistent by design, as marginalizing a Normal distribution boils down to relevant rows and columns of the covariance matrix and the corresponding elements of the mean vector. However, Gaussian Processes form a restrictive class of models, as any joint distribution of variables is Gaussian. To model more complex distributions, normalizing flows are a popular choice (Rezende and Mohamed, 2015).

**Separable Normalizing Flows.** Normalizing flows model distributions by transforming a source distribution  $p_Z$  on  $\mathbb{R}^K$  using an invertible transformation  $f: \mathbb{R}^K \rightarrow \mathbb{R}^K$ . Then the target distribution,

the distribution of the image of  $f$ , can be described by the transformation theorem for densities

$$p_Y(y) := p_Z(f^{-1}(y; \theta)) \cdot \left| \det \left( \frac{\partial f^{-1}(y; \theta)}{\partial y} \right) \right| \quad (7)$$

Existing approaches to normalizing flows use very simple source distributions, typically a multivariate standard normal  $p_Z(z) := \mathcal{N}(z \mid 0, \mathbb{I})$ , and model interactions between variables by means of the transformation (Rezende and Mohamed, 2015; Papamakarios et al., 2021). Current approaches for conditional normalizing flows for a variadic number of variables followed the same approach and tackled the problem by engineering expressive transformations between vectors of same size, for any size (Liu et al., 2019; Biloš and Günnemann, 2021; Yalavarthi et al., 2024b). For example, ProFITi uses an invertible attention mechanism. All these models in general will not have a guarantee for marginalization consistency. To the best of our knowledge, there is no simple condition on the transform that would provide such a guarantee.

We therefore propose a drastic change, reversing the standard approach for normalizing flows: to combine (i) simple, separable transforms with (ii) a richer source distribution, namely a Gaussian Process with full covariance matrix. This way interactions between variables can be represented by the covariance of the source distribution but not by transformation of source distribution.

**Lemma 4.1.** *A conditional flow model over  $\mathbb{R}^K$  or  $\text{Seq}(\mathbb{R})$  is separable, if it is expressed in the form*

$$f(z \mid Q, X) = (\phi(z_1 \mid Q_1, X), \dots, \phi(z_K \mid Q_K, X)) \quad (8)$$

for some univariate function  $\phi: \mathbb{R} \times \mathcal{Q} \times \text{Seq}(\mathcal{X}) \rightarrow \mathbb{R}$ , that is invertible in the first argument. Any model that consists of such a separable flow transformation, combined with a marginalization consistent model for the source distribution, is itself marginalization consistent. (Proof: Appendix A.1)

**Conditional Mixtures of Flows.** When using separably parametrized Gaussians as source distributions in Lemma 4.1, and expressive univariate transformations, we can model any kind of marginal as well as rich interactions between variables. However, the model is still restricted in its expressiveness, allowing for variable-wise separable transformations of a unimodal (Gaussian) distribution only. We therefore resort to the most simple way to further increase the expressiveness of the model: we combine several of such separable flows into a mixture. Figure 1 shows that even just a few components can lead to a much more expressive model, in particular comparable to a simple GMM without flow transformations (more details are provided in Appendix ??).

**Lemma 4.2.** *Given probabilistic models  $(\hat{p}_d)_{d=1:D}$  that satisfy **RI-R3**, then a mixture model*

$$\hat{p}(y \mid Q, X) = \sum_{d=1}^D w_d(X) \hat{p}_d(y \mid Q, X) \quad (9)$$

with permutation invariant weight function  $w: \text{Seq}(\mathcal{X}) \rightarrow \Delta^D$ , where  $\Delta^D$  denotes probability simplex in  $D$  variables:  $\Delta^D := \{w \in \mathbb{R}^D \mid w_d \geq 0, \sum_d w_d = 1\}$ , also satisfies **RI-R3**. (Proof: Appendix A.2)

## 5 Mixtures of Separable Flows (MOSES)

Based on the constructions from the last section, we propose to build a marginalization consistent model for forecasting irregular time series in four components (see Figure 2):

1. A separable encoder, consisting of
  - (i) A shared encoding  $\mathbf{h}^{\text{OBS}} := \text{enc}^{\text{OBS}}(X; \theta^{\text{OBS}})$  of the observations, used for all queries.
  - (ii)  $D$ -many encodings  $\mathbf{h}_{d,k} := \text{enc}^{\text{QRY}}(Q_k, X; \theta_d^{\text{QRY}})$  of each query and entire context.
2.  $D$ -many Gaussian Processes  $p_{Z_d}(z \mid \mu_d, \Sigma_d)$ , each separably parametrized according to (6), by the encoder for queries  $\mathbf{h}_d$ .
3.  $D$ -many separable normalizing flows  $\hat{p}_d^{\text{FLOW}}$ , one on top of each of the source distributions, whose transformations  $f_d$  are also separably parametrized by the encoded queries  $\mathbf{h}_d$ .
4. A mixture of the  $D$ -many normalizing flows with mixing weights  $w := w(\mathbf{h}^{\text{OBS}})$ , depending only on the encoded observations  $\mathbf{h}^{\text{OBS}}$ , but not the queries.

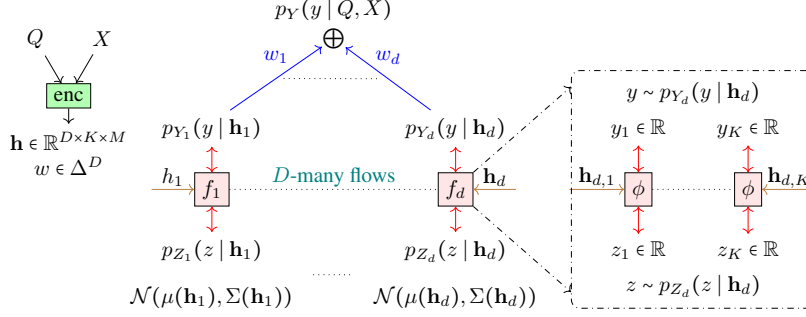


Figure 2: Illustration of MOSES.  $D$ -many flows (fixed).  $K$ -many variables (variable). Encoder (enc) takes  $X, Q$  (observed series and query timepoint-channel ids.) as input, and outputs an embedding  $\mathbf{h}$  (depends on both  $X$ , and  $Q$ ) and  $w$  (depends on  $X$  only).  $\mu, \Sigma$  of  $p_{Z_d}$  are parametrized by  $\mathbf{h}_d$ . Flow transformation of  $p_{Z_d}$ : parametrized by  $\mathbf{h}_d$ . Transformation layer:  $K$ -many univariate transformations  $\phi$  that transforms  $z_k$  of  $z \sim p_{Z_d}(z | \mathbf{h}_D)$  to  $y_k$  of  $y \sim p_d^{\text{FLOW}}(y | \mathbf{h}_d)$ .

**1. Separable Encoder.** To encode both the observations  $X = ((t_n^{\text{OBS}}, c_n^{\text{OBS}}, v_n^{\text{OBS}}))_{n=1:N}$  and queries  $Q = ((t_k^{\text{QRY}}, c_k^{\text{QRY}}))_{k=1:K}$ , we apply a positional embedding with learnable parameters  $(a_f, b_f)_{f=1:F}$  to the time component (Kazemi et al., 2019).

$$\text{pos\_embed}(t)_f := \begin{cases} a_f t + b_f & \text{if } f = 1 \\ \sin(a_f t + b_f) & \text{else} \end{cases} \quad (10)$$

And one-hot encodings for the channel component. The value is simply passed through.

$$\mathbf{x} := [\text{pos\_embed}(t_n^{\text{OBS}}), \text{one-hot}(c_n^{\text{OBS}}), v_n^{\text{OBS}}]_{n=1:N} \quad (11a)$$

$$\mathbf{q} := [\text{pos\_embed}(t_k^{\text{QRY}}), \text{one-hot}(c_k^{\text{QRY}})]_{k=1:K} \quad (11b)$$

The observations  $\mathbf{x} \in \mathbb{R}^{N \times (F+C+1)}$  are further encoded via self-attention and the queries  $\mathbf{q} \in \mathbb{R}^{K \times (F+C)}$  via cross-attention w.r.t. the encoded observations:

$$\mathbf{h}^{\text{OBS}} := \text{MHA}(\mathbf{x}, \mathbf{x}, \mathbf{x}; \theta^{\text{OBS}}) \quad (\in \mathbb{R}^{N \times M}) \quad (12a)$$

$$\tilde{\mathbf{h}} := \text{MHA}(\mathbf{q}, \mathbf{h}^{\text{OBS}}, \mathbf{h}^{\text{OBS}}; \theta^{\text{QRY}}) \quad (\in \mathbb{R}^{K \times D \cdot M}) \quad (12b)$$

$$\mathbf{h} := \text{reshape}(\tilde{\mathbf{h}}) \quad (\in \mathbb{R}^{D \times K \times M}) \quad (12c)$$

where MHA denotes multihead attention. For the encoding of the queries we use an encoding dimension  $D \cdot M$  and reshape each  $\mathbf{h}_k$  into  $D$  encodings  $\mathbf{h}_{d,k}$  of dimension  $M$ .

**2.  $D$  separably parametrized Gaussian source distributions  $p_{Z_d}(z | \mu_d, \Sigma_d)$ .** We model means and covariances simply by a linear and a quadratic function in the encoded queries  $\mathbf{h}_d$ :

$$\mu(\mathbf{h}_d) = \mathbf{h}_d \theta^{\text{MEAN}} \implies \mu(\mathbf{h}_d)_k = \mathbf{h}_{d,k} \theta^{\text{MEAN}} \quad (13a)$$

$$\begin{aligned} \Sigma(\mathbf{h}_d) &= \mathbb{I}_K + \frac{(\mathbf{h}_d \theta^{\text{COV}})(\mathbf{h}_d \theta^{\text{COV}})^T}{\sqrt{M'}} \\ &\implies \Sigma(\mathbf{h}_d)_{k,l} = \delta_{kl} + \frac{(\mathbf{h}_{d,k} \theta^{\text{COV}})(\mathbf{h}_{d,l} \theta^{\text{COV}})^T}{\sqrt{M'}} \end{aligned} \quad (13b)$$

where  $\theta^{\text{MEAN}} \in \mathbb{R}^{M \times 1}$  and  $\theta^{\text{COV}} \in \mathbb{R}^{M \times M'}$  are trainable weights shared across all  $D$  mixture components.  $\mathbb{I}_K$  is the  $K \times K$  identity matrix, and  $\delta_{kl} = 1$  if  $k = l$ , else 0, denotes the Kronecker delta. To ensure stable learning in (13b), we scale the inner product by  $\sqrt{M'}$ , following (Vaswani et al., 2017). Since  $\Sigma(\mathbf{h}_d)$  is the sum of a positive semi-definite and a positive definite matrix, it remains positive definite. Notably,  $\mathbf{h}_d$  encodes both context  $X$  and queries  $Q$ , assuming their roles in (6).

**3.  $D$  separable normalizing flows  $\hat{p}_d^{\text{FLOW}}$ .** To achieve separable invertible transformations, any univariate bijective functions can be applied on each variable separately. Spline based functions attracted interest due to their expressive and generalization capabilities (Durkan et al., 2019; Dolatabadi

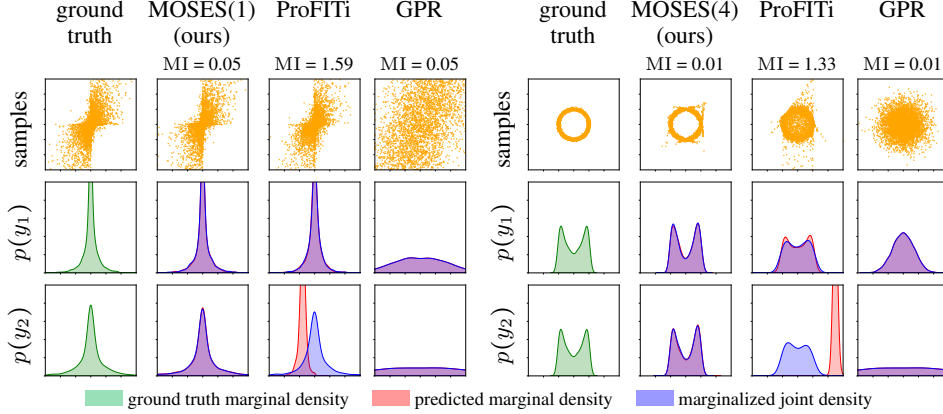


Figure 3: Demonstration of marginal consistency for MOSES (ours), ProFITi Yalavarthi et al. (2024b), and Gaussian Process Regression Bonilla et al. (2007) on two toy datasets: blast (left) and circle (right). ProFITi is inconsistent w.r.t. the marginals of the second variable  $y_2$ , while MOSES is consistent with the marginals of both  $y_1$  and  $y_2$ . MOSES( $D$ ) indicates  $D$  mixture components. Gaussian Process Regression (GPR) is marginalization consistent but predicts incorrect distributions.

et al., 2020). We employ computationally efficient Linear Rational Spline (LRS) transformations (Dolatabadi et al., 2020). For a conditional LRS  $\phi(z_k; \mathbf{h}_{d,k}, \theta^{\text{FLOW}})$ , the function parameters such as width and height of each bin, the derivatives at the knots, and  $\lambda$  are computed from the conditioning input  $\mathbf{h}_{d,k}$  and some model parameters  $\theta^{\text{FLOW}}$ .  $\theta^{\text{FLOW}}$  helps to project  $\mathbf{h}_{d,k}$  to the function parameters, and is common to all the variables  $z_{1:K}$  so that the transformation  $\phi$  can be applied for varying number of variables  $K$ . Note that we also share the same  $\theta^{\text{FLOW}}$  across all the  $D$ -many mixture components as well. For details, see Appendix A.4.

**4. Mixture Model.** We model the mixture weights via cross attention, using trainable parameters  $\beta \in \mathbb{R}^{D \times M}$  as attention queries, and a softmax to ensure the weights to sum to 1:

$$w := \text{softmax}(\text{MHA}(\beta, \mathbf{h}^{\text{OBS}}, \mathbf{h}^{\text{OBS}}; \theta^{\text{MIX}})) \quad (14)$$

**Theorem 5.1.** *Our model, MOSES, satisfies R1-R3 and hence realizes a stochastic process via Kolmogorov’s Extension Theorem (see Theorem 2.1). Proof. See Appendix A.3.*

**Computational Complexities.** The  $D$ -separable flows are computationally efficient: since they are separable, their Jacobian matrix is diagonal and computing determinant requires  $\mathcal{O}(K)$  operations. The main computational cost lies in evaluating  $\Sigma_d^{-1}$  and  $\det \Sigma_d^{-1}$  for the base distribution, which typically requires  $\mathcal{O}(K^3)$  operations. However, for large  $K$ , our low-rank modification  $\Sigma_d = \mathbb{I}_K + UU^T$  (see (13b)) reduces their computation to  $\mathcal{O}(M^2K)$  using the Woodbury and Weinstein–Aronszajn identities. This approach scales well for large values of  $K \gg M'$ , as  $M'$  is independent of  $K$ .

**Training.** Given a batch  $\mathcal{B}$  of training instances  $(Q, X, y)$ , we minimize the normalized joint negative log-likelihood (njNLL) (Yalavarthi et al., 2024b):

$$\mathcal{L}^{\text{njNLL}}(\theta) = \frac{1}{|\mathcal{B}|} \sum_{(Q, X, y) \in \mathcal{B}} -\frac{1}{|y|} \log \hat{p}(y | Q, X) \quad (15)$$

where  $\theta := (\theta^{\text{OBS}}, \theta^{\text{QRY}}, \theta^{\text{MIX}}, \theta^{\text{MEAN}}, \theta^{\text{COV}}, \theta^{\text{FLOW}})$ . njNLL generalizes NLL to dynamic size variables.

## 6 Experiments

### 6.1 Measuring Marginalization Consistency Violation

We assess how well a model’s predicted marginals match with those derived from its joint distribution using the **2-Wasserstein distance (WD)** or **Earth Movers Distance**. For each variable  $y_k$ , we compare:

Table 1: Comparing njNLL. Lower the better, best results in bold, second best in italics.

	Model	USHCN	Physionet'12	MIMIC-III	MIMIC-IV
inconsistent	ProFITi	$-3.226 \pm 0.225$	<b><math>-0.647 \pm 0.078</math></b>	<b><math>-0.377 \pm 0.032</math></b>	<b><math>-1.777 \pm 0.066</math></b>
consistent univariate	GRU-ODE	$0.766 \pm 0.159$	$0.501 \pm 0.001$	$0.961 \pm 0.064$	$0.823 \pm 0.318$
	NeuralFlows	$0.775 \pm 0.152$	$0.496 \pm 0.001$	$0.998 \pm 0.177$	$0.689 \pm 0.087$
	CRU	$0.761 \pm 0.191$	$1.057 \pm 0.007$	$1.234 \pm 0.076$	OOM
	Tripletformer+	$4.632 \pm 8.179$	$0.519 \pm 0.112$	$1.051 \pm 0.141$	$0.686 \pm 0.115$
consistent multivariate	GPR	$2.011 \pm 1.376$	$1.367 \pm 0.074$	$3.146 \pm 0.359$	$2.789 \pm 0.057$
	GMM	$1.050 \pm 0.031$	$1.063 \pm 0.002$	$1.160 \pm 0.020$	$1.076 \pm 0.003$
	MOSES (ours)	<b><math>-3.357 \pm 0.176</math></b>	<i><math>-0.491 \pm 0.041</math></i>	<i><math>-0.305 \pm 0.027</math></i>	<i><math>-1.668 \pm 0.097</math></i>

Table 2: Trained for njNLL and evaluate for mNLL, lower the better.

	Model	USHCN	Physionet'12	MIMIC-III	MIMIC-IV
inconsistent	ProFITi	$-3.324 \pm 0.206$	$-0.016 \pm 0.085$	$0.408 \pm 0.030$	$0.500 \pm 0.322$
consistent univariate	GRU-ODE	$0.776 \pm 0.172$	$0.504 \pm 0.061$	$0.839 \pm 0.030$	$0.876 \pm 0.589$
	Neural-Flows	$0.775 \pm 0.180$	$0.492 \pm 0.029$	$0.866 \pm 0.097$	$0.796 \pm 0.053$
	CRU	$0.762 \pm 0.180$	$0.931 \pm 0.019$	$1.209 \pm 0.044$	OOM
	Tripletformer+	$0.411 \pm 7.506$	$0.524 \pm 0.110$	$0.894 \pm 0.083$	$0.751 \pm 0.063$
consistent multivariate	GPR	-	-	-	-
	GMM	$1.042 \pm 0.021$	$1.069 \pm 0.002$	$1.124 \pm 0.007$	$1.075 \pm 0.007$
	MOSES (ours)	<b><math>-3.355 \pm 0.156</math></b>	<b><math>-0.271 \pm 0.028</math></b>	<b><math>0.163 \pm 0.026</math></b>	<b><math>-0.634 \pm 0.017</math></b>

- $\hat{p}(y_k | Q_k, X)$ : the predicted marginal,
- $\hat{p}^{\text{MAR}}(y_k | Q_k, X)$ : the marginal obtained by integrating the joint  $\hat{p}(y | Q, X)$ .

Since direct sampling from  $\hat{p}^{\text{MAR}}$  is difficult, we sample from the joint and extract the  $k$ -th component. The marginalization inconsistency is defined as the average WD across all  $K$  variables:

$$\text{MI} = \frac{1}{K} \sum_{k=1}^K \text{WD}(\hat{p}(y_k | Q_k, X), \hat{p}^{\text{MAR}}(y_k | Q_k, X)) \quad (16)$$

We use 1000 samples to compute the WD. Currently, we only use univariate marginals for computation. In principle, multivariate marginals could also be used, however they are computationally prohibitively expensive due to a lack of a closed form solution to compute the distance.

**Toy experiment.** We demonstrate that MOSES satisfies marginalization consistency using two synthetic bivariate distributions (Blast and Circle; see Figure 3, equations in Appendix B). The task is to estimate the unconditional joint distribution. MOSES accurately models both joint and marginal distributions while preserving consistency. In contrast, ProFITi captures the joint distribution well—especially for Blast—but fails on marginals due to its triangular attention mechanism, which enforces a fixed dependency order. GPR maintains consistency but lacks predictive accuracy.

## 6.2 Main experiment

We evaluate our model on four real-world datasets: one climate dataset (USHCN) and three medical datasets (Physionet'12, MIMIC-III, and MIMIC-IV). Following prior work (Yalavarthi et al., 2024b; Biloš et al., 2021), we observe the first 36h and predict the next 3 time steps for medical datasets, and observe 3 years and predict 3 time steps for USHCN. Both the number of observations ( $N$ ) and queries ( $K$ ) vary across samples (see Table 4). We split each dataset into training, validation, and test sets using a 70:10:20 ratio. We train MOSES using the Adam optimizer with a learning rate of 0.001 and batch size of 64. Hyperparameter search is over mixture components  $D \in 1, 2, 5, 7, 10$ , attention heads  $\in 1, 2, 4$ , and latent sizes  $M, F \in 16, 32, 64, 128$ . All models are implemented in PyTorch and trained on NVIDIA RTX 3090 and GTX 1080 Ti GPUs.

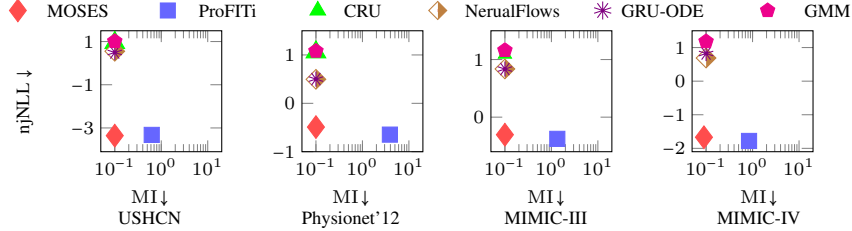


Figure 4: njNLL vs. MI. MOSES is marginalization consistent within sampling error.

Table 3: Comparing njNLL and mNLL across datasets to verify the contribution of probabilistic component of ProFITi. ‘ProFITi-TF‘ denotes ProFITi-Transformer using same encoder as MOSES

Dataset	njNLL		mNLL	
	ProFITi-TF	MOSES	ProFITi-TF	MOSES
USHCN	<b>-3.415±0.271</b>	-3.357±0.176	<b>-3.440±0.243</b>	-3.355±0.156
Physionet'12	<b>-0.657±0.034</b>	-0.491±0.041	0.017±0.042	<b>-0.271±0.028</b>
MIMIC-III	0.516±0.111	<b>-0.305±0.027</b>	1.279±0.057	<b>0.163±0.026</b>
MIMIC-IV	-1.405±0.220	<b>-1.668±0.097</b>	0.345±0.325	<b>-0.634±0.017</b>

**Baselines.** As baseline models, we use NeuralFlows (Biloš et al., 2021), GRU-ODE (De Brouwer et al., 2019), CRU (Schirmer et al., 2022), GPR (Dürichen et al., 2015), and ProFITi (Yalavarthi et al., 2024b). Our encoder is similar to Tripletformer (Yalavarthi et al., 2023) that predict marginal distributions for interpolation. We used it for the forecasting and called the model Tripletformer+. NeuralFlows, GRU-ODE, CRU, and Tripletformer+ predict only marginals and are marginalization consistent, as their joint distribution is the product of marginals. GPR is also marginalization consistent. We also compare with Gaussian Mixture Model (GMM) which is MOSES without flows attached to highlight the advantage of flows in MOSES.

**Results.** To highlight the importance of Marginalization Consistency in probabilistic forecasting models we train the model for njNLL in (16) and evaluate for two metrics: 1. Normalized Joint Negative Log-Likelihood (njNLL; Table 1) and 2. Marginal Negative Log-Likelihood (mNLL; Table 2). While njNLL measures the joint density of the predicted distribution, mNLL (Biloš et al., 2021; Schirmer et al., 2022) measures the univariate marginal density. An ideal probabilistic forecasting model should perform well on both metrics, ensuring not only accurate joint predictions but also in its marginal distributions. MOSES outperforms all marginalization-consistent models across both metrics. As expected, ProFITi is the best performing model for njNLL. MOSES performs comparably or slightly worse than ProFITi on njNLL. However, MOSES outperforms ProFITi significantly on mNLL. For USHCN, ProFITi and MOSES performs comparably, difference is within standard deviation. Figure 4 shows njNLL vs marginal inconsistency (MI). MOSES not only achieves similar likelihoods as ProFITi, its MI is close to 0 where ProFITi is up to an order of magnitude larger. Smaller values of MI for MOSES is due to sampling. We rounded the smaller MI to 0.1. This difference stems from ProFITi’s emphasis on learning joint distributions while overlooking marginalization consistency. When trained on large-scale joint distributions and later evaluated on a single query, ProFITi experiences notable performance degradation as observed in Figure 3. In contrast, MOSES maintains consistency, ensuring minimal loss in accuracy when queried for a single time-channel. Also, we note that the performance gains of ProFITi can be mostly attributed to its encoder. We experimented ProFITi and MOSES keeping same encoder (ProFITi-TF), and MOSES yields better accuracy than ProFITi in both MIMIC-III and MIMIC-IV (see Table 3).

**Consistency-Accuracy Trade-off.** While it may seem intuitive that enforcing marginalization consistency would improve the accuracy of probabilistic forecasts, this is not always the case. Marginalization consistency enhances the predictions’ reliability by ensuring coherence across marginals. However, achieving this often requires some modeling constraints that can slightly reduce accuracy. In critical domains such as healthcare, where trust and interpretability are crucial, the reliability afforded by consistent models is often more valuable than marginal accuracy gains.

## 7 Limitations

The primary limitation of MOSES lies in its structural constraints on both the encoder and the probabilistic component. These restrictions can lead to slight underperformance relative to ProFITi some times in modeling the joint distribution. This work represents an initial effort to address marginalization inconsistency, and we plan to enhance the model’s flexibility and performance in future. Additionally, Mixture weights cannot depend on query  $Q$ . It would seem intuitive to “switch-on”/“switch-off” certain components depending on the query time (i.e. short term vs long term forecast). However, **R1-R3** require the weights to be independent of  $Q$ .

## Conclusions

In this work, we propose MOSES: a marginalization-consistent mixture of separable flows for probabilistic forecasting of irregular time series with missing values. We demonstrate how to parametrize its components for decomposability and marginalization consistency. Experimental results on four real-world irregularly sampled time series datasets show that MOSES performs similarly to the state-of-the-art ProFITi model on joint distributions but significantly outperforms it on marginal distributions, highlighting the benefit of marginalization consistency.

## References

- Abdul Fatir Ansari, Alvin Heng, Andre Lim, and Harold Soh. Neural continuous-discrete state space models for irregularly-sampled time series. In Andreas Krause, Emma Brunskill, Kyunghyun Cho, Barbara Engelhardt, Sivan Sabato, and Jonathan Scarlett, editors, *Proceedings of the 40th International Conference on Machine Learning*, volume 202 of *Proceedings of Machine Learning Research*, pages 926–951. PMLR, 2023.
- Marin Biloš and Stephan Günnemann. Normalizing flows for permutation invariant densities. In Marina Meila and Tong Zhang, editors, *Proceedings of the 38th International Conference on Machine Learning*, volume 139 of *Proceedings of Machine Learning Research*, pages 957–967. PMLR, 2021.
- Marin Biloš, Johanna Sommer, Syama Sundar Rangapuram, Tim Januschowski, and Stephan Günnemann. Neural flows: Efficient alternative to neural ODEs. *Advances in Neural Information Processing Systems*, 34:21325–21337, 2021.
- Edwin V Bonilla, Kian Chai, and Christopher Williams. Multi-task gaussian process prediction. In *Advances in Neural Information Processing Systems*, volume 20, 2007.
- Zhengping Che, Sanjay Purushotham, Kyunghyun Cho, David Sontag, and Yan Liu. Recurrent neural networks for multivariate time series with missing values. *Scientific reports*, 8(1):1–12, 2018. doi: 10.1038/s41598-018-24271-9.
- Yuqi Chen, Kan Ren, Yansen Wang, Yuchen Fang, Weiwei Sun, and Dongsheng Li. ContiFormer: Continuous-time transformer for irregular time series modeling. *Advances in Neural Information Processing Systems*, 36, 2024.
- YooJung Choi, Antonio Vergari, and Guy Van den Broeck. Probabilistic Circuits: A Unifying Framework for Tractable Probabilistic Models\*. 2020.
- Sebastian Ciobanu. Mixtures of normalizing flows. In *Proceedings of ISCA 34th International Conference on Computer Applications in Industry and Engineering, EPIc Series in Computing*, volume 79, pages 82–90, 2021.
- Edward De Brouwer, Jaak Simm, Adam Arany, and Yves Moreau. GRU-ODE-Bayes: Continuous modeling of sporadically-observed time series. *Advances in Neural Information Processing Systems*, 32, 2019.
- Ruizhi Deng, Bo Chang, Marcus A Brubaker, Greg Mori, and Andreas Lehrmann. Modeling continuous stochastic processes with dynamic normalizing flows. In H. Larochelle, M. Ranzato, R. Hadsell, M.F. Balcan, and H. Lin, editors, *Advances in Neural Information Processing Systems*, volume 33, pages 7805–7815. Curran Associates, Inc., 2020.
- Laurent Dinh, Jascha Sohl-Dickstein, and Samy Bengio. Density estimation using real NVP. In *International Conference on Learning Representations*, 2017.

- Hadi Mohaghegh Dolatabadi, Sarah Erfani, and Christopher Leckie. Invertible generative modeling using linear rational splines. In *International Conference on Artificial Intelligence and Statistics*, pages 4236–4246. PMLR, 2020.
- Richard O. Duda and Peter E. Hart. Pattern classification and scene analysis. In *A Wiley-Interscience Publication*, 1974.
- Robert Dürichen, Marco A. F. Pimentel, Lei Clifton, Achim Schweikard, and David A. Clifton. Multitask gaussian processes for multivariate physiological time-series analysis. *IEEE Transactions on Biomedical Engineering*, 62(1):314–322, 2015. doi: 10.1109/TBME.2014.2351376.
- Conor Durkan, Artur Bekasov, Iain Murray, and George Papamakarios. Neural spline flows. *Advances in neural information processing systems*, 32, 2019.
- Max Horn, Michael Moor, Christian Bock, Bastian Rieck, and Karsten Borgwardt. Set functions for time series. In *International Conference on Machine Learning*, pages 4353–4363. PMLR, 2020.
- A Johnson, L Bulgarelli, T Pollard, S Horng, and LA Celi. Mark. R. *MIMIC-IV (version 1.0)*. *PhysioNet*, 2021.
- Alistair EW Johnson, Tom J Pollard, Lu Shen, Li-wei H Lehman, Mengling Feng, Mohammad Ghassemi, Benjamin Moody, Peter Szolovits, Leo Anthony Celi, and Roger G Mark. MIMIC-III, a freely accessible critical care database. *Scientific data*, 3(1):1–9, 2016.
- Seyed Mehran Kazemi, Rishab Goel, Sepehr Eghbali, Janahan Ramanan, Jaspreet Sahota, Sanjay Thakur, Stella Wu, Cathal Smyth, Pascal Poupart, and Marcus Brubaker. Time2Vec: Learning a Vector Representation of Time, July 2019. URL <http://arxiv.org/abs/1907.05321>. arXiv:1907.05321 [cs].
- Balaji Lakshminarayanan, Alexander Pritzel, and Charles Blundell. Simple and scalable predictive uncertainty estimation using deep ensembles. *Advances in Neural Information Processing Systems (NIPS)*, 30, 2017.
- Jenny Liu, Aviral Kumar, Jimmy Ba, Jamie Kiros, and Kevin Swersky. Graph normalizing flows. *Advances in Neural Information Processing Systems*, 32, 2019.
- Étienne Marcotte, Valentina Zantedeschi, Alexandre Drouin, and Nicolas Chapados. Regions of reliability in the evaluation of multivariate probabilistic forecasts. In *International Conference on Machine Learning*, pages 23958–24004. PMLR, 2023.
- Matthew J Menne, CN Williams Jr, and Russell S Vose. United States historical climatology network daily temperature, precipitation, and snow data. *Carbon Dioxide Information Analysis Center, Oak Ridge National Laboratory, Oak Ridge, Tennessee*, 2015.
- Kevin P. Murphy. *Probabilistic Machine Learning: An Introduction*. Adaptive Computation and Machine Learning Series. MIT Press, Cambridge, MA, USA, March 2022. ISBN 978-0-262-04682-4.
- Bernt Øksendal. *Stochastic Differential Equations*. Universitext. Springer, Berlin, Heidelberg, 2003. ISBN 978-3-540-04758-2 978-3-642-14394-6. doi: 10.1007/978-3-642-14394-6.
- George Papamakarios, Theo Pavlakou, and Iain Murray. Masked autoregressive flow for density estimation. In I. Guyon, U. Von Luxburg, S. Bengio, H. Wallach, R. Fergus, S. Vishwanathan, and R. Garnett, editors, *Advances in Neural Information Processing Systems*, volume 30. Curran Associates, Inc., 2017.
- George Papamakarios, Eric Nalisnick, Danilo Jimenez Rezende, Shakir Mohamed, and Balaji Lakshminarayanan. Normalizing flows for probabilistic modeling and inference. *Journal of Machine Learning Research*, 22(1), January 2021. ISSN 1532-4435.
- Guilherme G. P. Freitas Pires and Mário A. T. Figueiredo. Variational mixture of normalizing flows. In *28th European Symposium on Artificial Neural Networks, Computational Intelligence and Machine Learning, ESANN 2020, Bruges, Belgium, October 2-4, 2020*, pages 205–210, 2020.
- Janis Postels, Mengya Liu, Riccardo Spezialetti, Luc Van Gool, and Federico Tombari. Go with the flows: Mixtures of normalizing flows for point cloud generation and reconstruction. In *2021 International Conference on 3D Vision (3DV)*, pages 1249–1258. IEEE, 2021. doi: 10.1109/3DV53792.2021.00132.

- Kashif Rasul, Abdul-Saboor Sheikh, Ingmar Schuster, Urs M Bergmann, and Roland Vollgraf. Multivariate probabilistic time series forecasting via conditioned normalizing flows. In *International Conference on Learning Representations*, 2021.
- Danilo Rezende and Shakir Mohamed. Variational Inference with Normalizing Flows. In *International Conference on Machine Learning*, pages 1530–1538. PMLR, June 2015.
- Mona Schirmer, Mazin Eltayeb, Stefan Lessmann, and Maja Rudolph. Modeling irregular time series with continuous recurrent units. In *Proceedings of the 39th International Conference on Machine Learning*, volume 162, pages 19388–19405. PMLR, 2022.
- Maximilian Seitzer, Arash Tavakoli, Dimitrije Antic, and Georg Martius. On the Pitfalls of Heteroscedastic Uncertainty Estimation with Probabilistic Neural Networks. In *International Conference on Learning Representations*, 2021.
- Marcin Sendera, Jacek Tabor, Aleksandra Nowak, Andrzej Bedychaj, Massimiliano Patacchiola, Tomasz Trzcinski, Przemysław Spurek, and Maciej Zieba. Non-gaussian gaussian processes for few-shot regression. *Advances in Neural Information Processing Systems*, 34:10285–10298, 2021.
- Satya Narayan Shukla and Benjamin Marlin. Heteroscedastic temporal variational autoencoder for irregularly sampled time series. In *International Conference on Learning Representations*, 2022.
- Sahil Sidheekh, Kristian Kersting, and Sriraam Natarajan. Probabilistic Flow Circuits: Towards Unified Deep Models for Tractable Probabilistic Inference. In *Proceedings of the Thirty-Ninth Conference on Uncertainty in Artificial Intelligence*, pages 1964–1973. PMLR, July 2023.
- Ikaro Silva, George Moody, Daniel J Scott, Leo A Celi, and Roger G Mark. Predicting in-hospital mortality of icu patients: The physionet/computing in cardiology challenge 2012. In *2012 Computing in Cardiology*, pages 245–248. IEEE, 2012.
- Ashish Vaswani, Noam Shazeer, Niki Parmar, Jakob Uszkoreit, Llion Jones, Aidan N Gomez, Łukasz Kaiser, and Illia Polosukhin. Attention is all you need. *Advances in Neural Information Processing Systems*, 30, 2017.
- Vijaya Krishna Yalavarthi, Johannes Burchert, and Lars Schmidt-Thieme. Tripletformer for Probabilistic Interpolation of Irregularly sampled Time Series. *2023 IEEE International Conference on Big Data (Big Data)*, 2023.
- Vijaya Krishna Yalavarthi, Kiran Madhusudhanan, Randolph Scholz, Nourhan Ahmed, Johannes Burchert, Shayan Jawed, Stefan Born, and Lars Schmidt-Thieme. GraFITi: Graphs for Forecasting Irregularly Sampled Time Series. In Michael J. Wooldridge, Jennifer G. Dy, and Sriraam Natarajan, editors, *Thirty-Eighth AAAI Conference on Artificial Intelligence, AAAI 2024, February 20-27, 2024, Vancouver, Canada*, pages 16255–16263. AAAI Press, 2024a. doi: 10.1609/AAAI.V38I15.29560.
- Vijaya Krishna Yalavarthi, Randolph Scholz, Stefan Born, and Lars Schmidt-Thieme. Probabilistic forecasting of irregular time series via conditional flows. *CoRR*, abs/2402.06293, 2024b. doi: 10.48550/ARXIV.2402.06293.

## A Theory

### A.1 Proof of Lemma 4.1

*Proof.* Since  $X$  is a common conditional to all the marginals, we can ignore it. So, assume that  $f$  is a separable transformation:

$$f(z | Q) = (\phi(z_1 | Q_1), \dots, \phi(z_K | Q_K)) \quad (17)$$

and that  $\hat{p}_Z(z | Q)$  is marginalization consistent model. Then, the predictive distribution is

$$\hat{p}(y | Q) = \hat{p}_Z(f^{-1}(y | Q) | Q) \cdot \left| \det \frac{df^{-1}(y | Q)}{dy} \right| \quad (18)$$

Since  $f$  is separable, it follows that the Jacobian is diagonal:

$$\begin{aligned} \frac{df^{-1}(y | Q)}{dy} &= \frac{d(\phi^{-1}(y_1 | Q_1), \dots, \phi^{-1}(y_K | Q_K))}{d(y_1, \dots, y_K)} \\ &= \text{diag} \left( \frac{d\phi^{-1}(y_1 | Q_1)}{dy_1}, \dots, \frac{d\phi^{-1}(y_K | Q_K)}{dy_K} \right) \end{aligned} \quad (19)$$

Hence, the determinant of the Jacobian is the product of the diagonal elements:

$$\left| \det \frac{df^{-1}(y | Q)}{dy} \right| = \prod_{k=1:K} \left| \det \frac{d\phi^{-1}(y_k | Q_k)}{dy_k} \right| = \prod_{k=1:K} \left| \frac{d\phi^{-1}(y_k | Q_k)}{dy_k} \right| \quad (20)$$

Using this fact, we can integrate the joint density over  $y_k$  to get the marginal density:

$$\begin{aligned} & \int \hat{p}(y | Q) dy_k \\ &= \int \hat{p}_Z(f^{-1}(y | Q) | Q) \cdot \left| \det \frac{df^{-1}(y | Q)}{dy} \right| dy_k \quad \triangleright (7) \\ &= \int \hat{p}_Z(f^{-1}(y | Q) | Q) \cdot \prod_{k=1:K} \left| \frac{d\phi^{-1}(y_k | Q_k)}{dy_k} \right| dy_k \quad \triangleright (20) \\ &= \left( \prod_{l \neq k} \left| \frac{d\phi^{-1}(y_l | Q_l)}{dy_l} \right| \right) \cdot \int \hat{p}_Z(f^{-1}(y | Q) | Q) \cdot \left| \frac{d\phi^{-1}(y_k | Q_k)}{dy_k} \right| dy_k \\ &= \left( \prod_{l \neq k} \left| \frac{d\phi^{-1}(y_l | Q_l)}{dy_l} \right| \right) \cdot \int \hat{p}_Z(z | Q) dz_k \quad \triangleright \text{transf.-thm} \\ &= \left( \prod_{l \neq k} \left| \frac{d\phi^{-1}(y_l | Q_l)}{dy_l} \right| \right) \hat{p}_Z(z_{-k} | Q_{-k}) \quad \triangleright (5) \\ &= \hat{p}_Z(z_{-k} | Q_{-k}) \left| \det \frac{df^{-1}(y_{-k} | Q_{-k})}{dy_{-k}} \right| \quad \triangleright (20) \\ &= \hat{p}(y_{-k} | Q_{-k}) \quad \triangleright (7) \end{aligned}$$

□

## A.2 Proof of Lemma 4.2

*Proof.* Consider a mixture model of the form

$$\hat{p}(y | Q, X) := \sum_{d=1}^D w_d(X) \hat{p}_d(y | Q, X) \quad (21)$$

satisfying the conditions from Lemma 4.2, i.e. the component models  $\hat{p}_d$  satisfy the requirements **R1**–**R3** and the weight function  $w: \text{Seq}(\mathcal{X}) \rightarrow \Delta^D$  is permutation invariant with respect to  $X$ .

1.  $\hat{p}$  satisfies **R1**: By construction of the mixture model, it has the same domain and codomain as the component models.
2.  $\hat{p}$  satisfies **R2**: Let  $\pi \in S_{|Q|}$  and  $\tau \in S_{|X|}$ , then

$$\begin{aligned} \hat{p}(y | Q^\pi, X^\tau) &= \sum_{d=1}^D w_d(X^\tau) \hat{p}_d(y | Q^\pi, X^\tau) \\ &= \sum_{d=1}^D w_d(X) \hat{p}_d(y | Q, X) \\ &\quad \triangleright \text{permutation invariance of } w \text{ and } \hat{p}_d \\ &= \hat{p}(y | Q, X) \end{aligned}$$

3.  $\hat{p}$  satisfies **R3**:

$$\begin{aligned} \int \hat{p}(y | Q, X) dy_k &= \int \sum_{d=1}^D w_d(X) \hat{p}_d(y | Q, X) dy_k \\ &= \sum_{d=1}^D w_d(X) \int \hat{p}_d(y | Q, X) dy_k \\ &= \sum_{d=1}^D w_d(X) \hat{p}_d(y_{-k} | Q_{-k}, X) \quad \triangleright \hat{p}_d \text{ is marginalization consistent} \\ &= \hat{p}_Y(y_{-k} | Q_{-k}, X) \end{aligned}$$

□

### A.3 Proof of Theorem 5.1

*Proof.* Due to Lemma 1, it is sufficient to show that all the component models satisfy the requirements **R1-R3**. Since we use Gaussian Processes as the base distribution, Lemma 4.1 ensures that each component model is marginalization consistent, establishing **R3**. Requirement **R1** is by construction. Finally, permutation invariance **R2** can be seen as follows:

First, note that, by Equation (12), it follows that if  $\mathbf{h}^{\text{OBS}}$  is permutation equivariant with respect to  $X$ , and  $\tilde{\mathbf{h}}$  and  $\mathbf{h}$  are both permutation equivariant with respect to  $Q$  and permutation invariant with respect to  $X$ . Now, let  $\pi \in S_{|Q|}$  and  $\tau \in S_{|X|}$ , then, for the  $d$ -th component model  $\hat{p}_{Y_d}(y | Q, X)$ . In particular, the flow satisfies  $f_d^{-1}(y^\pi, Q^\pi, X^\tau) = f^{-1}(y^\pi, \mathbf{h}_d^\pi) = z^\pi$ . Therefore:

$$\begin{aligned}
& \hat{p}_{Y_d}(y^\pi | Q^\pi, X^\tau) \\
&= \hat{p}_{Z_d}(f^{-1}(y^\pi, Q^\pi, X^\tau) | Q^\pi, X^\tau) \cdot \left| \det \frac{df^{-1}(y^\pi, Q^\pi, X^\tau)}{dy^\pi} \right| \\
&= \mathcal{N}(f^{-1}(y^\pi, \mathbf{h}_d^\pi) | \mu(\mathbf{h}_d^\pi), \Sigma(\mathbf{h}_d^\pi)) \cdot \left| \det \frac{df^{-1}(y^\pi, \mathbf{h}^\pi)}{dy^\pi} \right| \quad \triangleright \text{by remark above} \\
&= \mathcal{N}(z^\pi | \mu(\mathbf{h}_d^\pi), \Sigma(\mathbf{h}_d^\pi)) \cdot \left| \det \frac{df^{-1}(y^\pi, \mathbf{h}^\pi)}{dy^\pi} \right| \\
&= \mathcal{N}(z | \mu, \Sigma) \cdot \left| \det \frac{df^{-1}(y^\pi, \mathbf{h}^\pi)}{dy^\pi} \right| \quad \triangleright \text{permutation invariance of GP} \\
&= \mathcal{N}(z | \mu, \Sigma) \cdot \left| \det \frac{df^{-1}(y, \mathbf{h})}{dy} \right| \quad \triangleright \text{by (20)} \\
&= \hat{p}_{Y_d}(y | Q, X)
\end{aligned}$$

□

### A.4 Linear Rational Splines

Linear Rational Splines (LRS) are computationally efficient spline functions Dolatabadi et al. (2020). Formally, given a set of monotonically increasing points  $\{(u_m, v_m)\}_{m=1:M}$  called knots, that is  $u_m < u_{m+1}$  and  $v_m < v_{m+1}$ , along with their corresponding derivatives  $\{\Delta_m > 0\}_{m=1:M}$ , then the LRS transformation  $\phi(u)$  within a bin  $u \in [u_m, u_{m+1}]$  is:

$$\phi(u) = \begin{cases} \frac{\alpha_m v_m (\lambda_m - \tilde{u}) + \bar{\alpha}_m \bar{v}_m \tilde{u}}{\alpha_m (\lambda_m - \tilde{u}) + \bar{\alpha}_m \tilde{u}} & : 0 \leq \tilde{u} \leq \lambda_m \\ \frac{\bar{\alpha}_m \bar{v}_m (1 - \tilde{u}) + \alpha_{m+1} v_{m+1} (\tilde{u} - \lambda_m)}{\bar{\alpha}_m (1 - \tilde{u}) + \alpha_{m+1} (\tilde{u} - \lambda_m)} & : \lambda_m \leq \tilde{u} \leq 1 \end{cases}$$

where  $\tilde{u} = \frac{u - u_m}{u_{m+1} - u_m} \in [0, 1]$  (22)

Here,  $\lambda_m \in (0, 1)$  signifies the location of automatically inserted virtual knot between  $u_m$  and  $u_{m+1}$  with value  $\bar{v}_m$ . The values of  $\lambda_m$ ,  $\alpha_m$ ,  $\bar{\alpha}_m$  and  $\bar{v}_m$  are all automatically derived from the original knots and their derivatives Dolatabadi et al. (2020). For a conditional LRS  $\phi(z_k; \mathbf{h}_{d,k}, \theta)$ , the function parameters such as width and height of each bin, the derivatives at the knots, and  $\lambda$  are computed from the conditioning input  $\mathbf{h}_{d,k}$  and some model parameters  $\theta$ .  $\theta$  helps to project  $\mathbf{h}_{d,k}$  to the function parameters, and is common to all the variables  $z_{1:K}$  so that the transformation  $\phi$  can be applied for varying number of variables  $K$ . Additionally, we set  $\theta$  common to all the components as well. Since, each component has separate embedding for a variable  $z_k$  ( $\mathbf{h}_{d,k}$ ), we achieve different transformations in different components for same variable.

In summary, the conditional flow model is separable across the query size  $f = f_1 \times \dots \times f_K$  with

$$f_d(y) := f(y | \mathbf{h}_d) = (\phi(y_1, \mathbf{h}_{d,1}), \dots, \phi(y_K, \mathbf{h}_{d,K})) \quad (23)$$

Table 4: Statistics of the datasets used in our experiments. Sparsity means the percentage of missing observations in the time series.  $N$  is the total number of observations and  $K$  is the number of queries in our experiments in Section 6.

Name	#Samples	#Channels	Sparsity	N	K
USHCN	1100	5	77.9%	8 – 322	3 – 6
PhysioNet’12	12,000	37	85.7%	3 – 519	1 – 53
MIMIC-III	21,000	96	94.2%	4 – 709	1 – 85
MIMIC-IV	18,000	102	97.8%	1 – 1382	1 – 79

Table 5: Comparing models w.r.t. MSE. Lower the better.

Model	USHCN	PhysioNet’12	MIMIC-III	MIMIC-IV
GRU-ODE	0.410 ± 0.106	0.329 ± 0.004	<b>0.479 ± 0.044</b>	0.365 ± 0.012
Neural-Flows	0.424 ± 0.110	0.331 ± 0.006	<b>0.479 ± 0.045</b>	0.374 ± 0.017
CRU	<b>0.290 ± 0.060</b>	0.475 ± 0.015	0.725 ± 0.037	OOM
Tripletformer+	0.349 ± 0.131	<b>0.293 ± 0.018</b>	0.547 ± 0.068	0.369 ± 0.030
ProFITi	0.308 ± 0.061	0.305 ± 0.007	0.548 ± 0.063	0.389 ± 0.015
MOSES (ours)	0.411 ± 0.099	0.307 ± 0.006	0.517 ± 0.057	<b>0.342 ± 0.028</b>

## B Datasets

4 real-world datasets are used in the experiments.

**USHCN Menne et al. (2015).** This is a climate dataset consisting of 5 climate variables such as daily temperatures, precipitation and snow measured over 150 years at 1218 meteorological stations in the USA. Following De Brouwer et al. (2019); Yalavarthi et al. (2024b), we selected 1114 stations and an observation window of 4 years from 1996 until 2000.

**PhysioNet2012 Silva et al. (2012).** This physiological dataset consists of the medical records of 12,000 patients who are admitted into ICU. 37 vitals are recorded for 48 hrs. Following the protocol of Yalavarthi et al. (2024a); Che et al. (2018), dataset consists of hourly observations in each series.

**MIMIC-III Johnson et al. (2016).** This is also a physiological dataset. It is a collection of readings of the vitals of the patients admitted to ICU at Beth Israeli Hospital. Dataset consists of 18,000 instances and 96 variables are measured for 48 hours. Following De Brouwer et al. (2019); Biloš et al. (2021); Yalavarthi et al. (2024b) observations are rounded to 30 minute intervals.

**MIMIC-IV Johnson et al. (2021).** The successor of the MIMIC-III dataset. Here, 102 variables from patients admitted to ICU at a tertiary academic medical center in Boston are measured for 48 hours. Following De Brouwer et al. (2019); Biloš et al. (2021); Yalavarthi et al. (2024b) observations, are rounded to 1 minute intervals.

**Blast distribution (toy dataset).** Blast distribution is a bivariate distribution which is created as follows:

$$z \sim \mathcal{N}\left(\begin{bmatrix} 0 \\ 0 \end{bmatrix}, \begin{bmatrix} 1 & 1 \\ 1 & 2 \end{bmatrix}\right)$$

$$y = \text{sign}(z) \odot z \odot z$$

**Circle (toy dataset).** Circle is also a bi-variate distribution.

$$z \sim \mathcal{N}(0, \mathbb{I}_2)$$

$$y = \frac{z}{\|z\|_2} + 0.05 \cdot \mathcal{N}(0, \mathbb{I}_2)$$

Table 6: Experiment on varying observation and forecast horizons. Evaluation metric-njNLL, Lower the better

	36/12	24/24	12/36
ProFITi	<b>-0.768±0.041</b>	<b>-0.355±0.243</b>	<b>-0.291±0.415</b>
MOSES (ours)	-0.315±0.016	-0.298±0.027	-0.063±0.049

Table 7: Experiment on varying observation and forecast horizons. Evaluation metric-mNLL, Lower the better

	36/12	24/24	12/36
ProFITi	1.376±1.764	0.705±0.179	2.977±2.978
MOSES (ours)	<b>-0.083±0.025</b>	<b>-0.020±0.060</b>	<b>0.040±0.131</b>

## C Additional Experiments

### C.1 Comparing for Point Forecasting

While point forecasting is an important task in time series analysis, the goal of probabilistic forecasting is fundamentally different. Probabilistic forecasting aims to capture the full predictive distribution rather than just a single-point estimate. Nonetheless, one might intuitively expect that the best probabilistic model would also yield the most accurate point estimates. However, this is not always the case in practice, as noted in prior works (Lakshminarayanan et al., 2017; Seitzer et al., 2021; Rasul et al., 2021; Yalavarthi et al., 2024b).

We compare probabilistic models in terms of point prediction accuracy using Mean Squared Error (MSE), as reported in Table 5. Our results show that no single model consistently outperforms the others across all datasets. We believe there are two primary reasons for this phenomenon:

- (1.) MSE is related to the Negative Log-Likelihood (NLL) of a Gaussian distribution with a fixed standard deviation. Therefore, models explicitly trained by minimizing Gaussian Negative Log-Likelihood (even if they predict more than just the mean) are naturally optimized for this metric.
- (2.) Probabilistic models are trained to predict the underlying data distribution, not solely the optimal point estimate (e.g., the conditional mean). Their objective is to accurately capture the uncertainty and dependencies in the data, which involves learning the (co)variance structure. This focus on the full distribution can sometimes lead to point estimates that are not strictly optimized for minimizing the squared error, even if the overall probabilistic forecast is superior.

Except for MOSES and ProFITi, all the other probabilistic models are designed to predict Gaussian distributions. Between ProFITi and MOSES, their performance is comparable. ProFITi outperforms MOSES on the USHCN whereas MOSES performs better in MIMIC-IV. For, Physionet’12 and MIMIC-III they have comparable performances (difference is within standard deviation).

### C.2 Experiment on varying observation and forecast horizons

We would like to see if MOSES is scalable to long observations and forecast horizons. For this, we performed an experiment on varying length observation and forecasting horizons on Physionet’12 dataset and compared against the published results from (Yalavarthi et al., 2024b) in Table 6. The observation and forecasting horizons are: {(36h, 12h), (24h, 36h), (12h, 26h)}.

Table 8: Comparing for Energy Score. Lower the better

	USHCN	PhysioNet’12	MIMIC-III	MIMIC-IV
NeuralFlows	0.661 ± 0.059	1.691 ± 0.001	1.381 ± 0.033	0.982 ± 0.009
ProFITi	<b>0.452 ± 0.044</b>	<b>0.879 ± 0.303</b>	1.606 ± 0.168	<b>0.808 ± 0.003</b>
MOSES	0.552 ± 0.044	1.599 ± 0.013	<b>1.353 ± 0.033</b>	0.906 ± 0.029

Table 9: Comparing models w.r.t. CRPS score on marginals. Lower the better.

Model	USHCN	PhysioNet'12	MIMIC-III	MIMIC-IV
Neural-flows	0.306 ± 0.028	0.277 ± 0.003	0.308 ± 0.004	0.281 ± 0.004
ProFITi	<b>0.182 ± 0.007</b>	0.271 ± 0.003	0.319 ± 0.003	0.279 ± 0.012
MOSES (ours)	0.220 ± 0.019	<b>0.260 ± 0.002</b>	<b>0.296 ± 0.005</b>	<b>0.245 ± 0.010</b>

Table 10: Ablation study on PhysioNet2012

Model	njNLL (↓)
MOSES	-0.491 ± 0.041
MOSES- <i>f</i>	1.063 ± 0.002
MOSES-coV	-0.308 ± 0.024
MOSES- <i>w</i>	-0.451 ± 0.038
MOSES (1)	-0.493 ± 0.029

Tables 6 and 7 present the njNLL and mNLL results for ProFITi and MOSES. The results follow the trends observed in Tables 1 and 2. ProFITi performs best when predicting joint distributions. However, its lack of marginalization consistency leads to a severe performance drop when predicting marginal distributions. In contrast, MOSES maintains stable performance from njNLL to mNLL. While it performs slightly worse than ProFITi on njNLL, it significantly outperforms ProFITi on mNLL.

### C.3 Comparing for Energy Score

The Energy Score between the ground truth  $y$  and predicted distribution  $\hat{p}_Y$  is computed as:

$$ES(y, \hat{p}_Y) := \mathbb{E}_{y' \sim \hat{p}_Y} \|y - y'\|_2^p - \frac{1}{2} \mathbb{E}_{y', y'' \sim \hat{p}_Y} \|y' - y''\|_2^p, \quad (24)$$

where  $\|\cdot\|_2$  denotes the Euclidean norm and  $p \in (0, 2)$  is a parameter. In our evaluation, we set  $p = 1$ . Marcotte et al. (2023) demonstrated that the Energy Score is not a reliable metric for evaluating multivariate distributions. Additionally, it suffers from the curse of dimensionality, as it requires  $N^K$  samples, where  $K$  is the number of variables and  $N$  is the number of samples required to accurately estimate a univariate distribution.

However, since many regularly sampled, fully observed multivariate time series probabilistic forecasting models use the Energy Score as an evaluation metric, we examine how MOSES compares to the best-performing inconsistent multivariate probabilistic model, ProFITi, and the consistent univariate probabilistic model, NeuralFlows in Table 8. Our results show that MOSES outperforms NeuralFlows across all datasets. As shown by the njNLL metric in Table 1, ProFITi is the best-performing model, outperforming MOSES in 3 out of 4 datasets.

### C.4 Comparing for Marginals in Terms of CRPS

We compare with CRPS score in Table 9, a widely used evaluation metric in time series forecasting. We see that MOSES outperforms all the consistent models. It performs better than ProFITi in 3 out of 4 dataset. For ProFITi and MOSES, we sampled 1000 instances and computed the CRPS.

Table 11: Comparing the number of parameters and run-time per epoch for results in Table 1 for GMM and MOSES, and ProFITi for reference

	USHCN		Physionet'12		MIMIC-III		MIMIC-IV	
	Parameters	Run Time	Parameters	Run Time	Parameters	Run Time	Parameters	Run Time
ProFITi	1,093.0K	3.8s	75.8K	42.14s	59.7K	66.8s	285.9K	70.2s
GMM	416.0K	0.9s	390.9K	5.9s	33.0K	18.5s	101.1K	21.3s
MOSES (ours)	167.6K	2.4s	134.6K	14.1s	112.6K	25.4s	398.6K	33.3s

### C.5 Ablation study.

Using Physionet’12, we show the importance of different model components. As summarized in Table 10, the performance is reduced by removing the flows (MOSES –  $f$ ) which is same as GMM. It is expected that normalizing flows are more expressive compared to simple mixture of Gaussians. On the other hand, by using only isotropic Gaussian as the base distribution (MOSES – COV) model performance worsened. Similarly, parameterizing the components weights have a slight advantage over fixing them to  $1/D$  with  $D$  being the number of components. One interesting observation is even using single component (MOSES(1)) gives similar results compared to mixture of such components. This could be because the dataset we have may not require multiple components. We note that we have  $D = 1$  in our hyperparameter space, and we select the best  $D$  based on validation dataset.

### C.6 Comparing the number of parameters and runtime for GMM and MOSES

Since MOSES is built upon GMM, Table 11 presents the number of parameters and runtime for both MOSES and GMM. For reference, we also include ProFITi.

The results show that GMM has a relatively low number of parameters for MIMIC-III and MIMIC-IV, whereas for USHCN and PhysioNet’12, the number of parameters is significantly higher. The primary difference between GMM and MOSES is the inclusion of flows. Given that all other factors remain the same, MOSES is expected to have a slightly higher number of parameters than GMM due to these additional flows. Also, the parameters for the flows are shared among all the variables and the components, their number does not grow with increase in components or variables. However, differences in the chosen hyperparameters for GMM and MOSES lead to some discrepancies from this expectation. Moreover, the inclusion of flows in MOSES results in a slightly higher runtime compared to GMM.